Layer-Thinning Effects on Ferroelectricity and the Ferroelectric-to-Paraelectric Phase Transition of Vinylidene Fluoride−Trifluoroethylene Copolymer Layers

Kenji Urayama,† Masaki Tsuji,‡ and Dieter Neher*,§

Max-Planck-Institut für Polymerforschung, Ackermannweg 10, D-55128 Mainz, Germany, and Institute for Chemical Research, Kyoto University, Uji, Kyoto-fu 611-0011, Japan

Received May 17, 2000; Revised Manuscript Received August 31, 2000

ABSTRACT: Dielectric and electromechanical properties of vinylidene fluoride−trifluoroethylene copolymer layers with thickness ranging from 1300 nm down to 65 nm have been investigated by dielectric spectroscopy and electromechanical interferometry. The effects of layer thickness (h) on ferroelectricity and the ferroelectric-to-paraelectric phase transition are discussed on the basis of the temperature (T) dependence of the dielectric constant (ϵ) and electrostrictive and inverse-piezoelectric effects. In the region of h less than a few hundred nanometers, the layer-thinning effect on ϵ becomes prominent, and ϵ decreases with a decrease in h, but the phase transition temperature (T_c) and the Curie constants are not significantly influenced by layer thinning. The dependence of the electrostriction on the square of the applied electric field for unpoled films is nonlinear in the ferroelectric phase, while it is linear in the paraelectric phase. The degree of the nonlinearity decreases as the layer becomes thinner, and for a 65 nm thick film the nonlinearity almost vanishes at temperatures fairly below T_c. Remanent polarizations (P_r) achieved by poling are ca. 55 mC/m^2 for the films of $h \geq 90$ nm, while P_r for the 65 nm thick film (40 mC/m^2) is definitely lower. Differential scanning calorimetry shows that the degree of crystallinity (fraction of ferroelectric crystalline phase) decreases with reduction in film thickness, and especially the crystallinity for the 65 nm thick film is much lower than those for the thicker ones. In comparison, between the 1300 and 65 nm thick films, the reduction in the degree of crystallinity is comparable to the decrease in P_r. The variation of the dielectric constant and the degree of crystallinity on h are reasonably well explained assuming the presence of a nonferroelectric amorphous-like surface near layer. Electron microscopic studies of the 65 nm thick layer suggest a preferred orientation of the chain axis of the crystallites parallel to the film surface. The presence of the preferential crystalline orientation might as well explain the appreciably different values of the surface near layer thickness (12 and 27 nm) evaluated from the h dependence of the dielectric constant and the degree of crystallinity. The layer thickness dependence of the dielectric and electromechanical properties is interpreted as a result of a combined effect of the reduction in degree of crystallinity and the specific crystallite orientation due to layer thinning.

Introduction

The ferroelectric-to-paraelectric phase transition of crystalline copolymers of vinylidene fluoride and trifluoroethylene [P(VDF-TrFE)] has been extensively examined[1−8] over the past two decades since Yagi et al.[9] showed that the copolymers with more than 50 mol % VDF content have a definite Curie temperature. P(VDF-TrFE) has also been studied as a promising ferroelectric material due to the strong piezoelectricity and pyroelectricity, and the ferroelectric properties have been widely investigated.[10−15] Most of the earlier studies have treated the P(VDF-TrFE) films with a thickness of 10 μm or more. Thin copolymer films with layer thickness well below 1 μm have potential application in optical and acoustical technologies.[16] Also, those ultrathin copolymer layers represent interesting systems to study the ferroelectric-to-paraelectric phase transition as well as the ferroelectricity in a reduced-dimension system. The phase transition behavior of ca. 1 μm thick P(VDF-TrFE) films was shown to be essentially the same as that of thicker ones by dielectric[17,18] and electromechanical[18] measurements. Bune et al.[19] reported that bulklike ferroelectric properties was observed even in films of only two monolayers (equivalent to a thickness of 1 nm) of 70 mol % VDF copolymer fabricated by the Langmuir−Blodgett technique. They also found that the phase transition temperature is nearly equal to the bulk value even in the ultrathin LB films.[19] Bune et al.[19−22] and Kimura et al.[23] showed that the coercive electric fields were much larger in the LB copolymer film[19−22] and a spin-coated 60 nm thick copolymer film[23] than thicker films, though these thin films exhibited a high ability of polarization by poling. The pyroelectric and piezoelectric coefficients of a 35 nm thick LB films were measured to be approximately 50% of that of a spun film of the same material.[22] However, the details of the layer-thinning effects on the ferroelectric properties and the phase transition (such as the layer thickness dependence) including the physical origin of the layer-thinning effects have still remained incompletely characterized and understood.

In the present study, we have investigated dielectric and electromechanical properties of a thin spin-coated P(VDF-TrFE) layer with a thickness ranging from 1.3 μm down to 65 nm as a function of temperature. Electrostriction and inverse-piezoelectric effects of the thin copolymer layers have been measured by an electromechanical interferometer. It has been demonstrated that this technique is very useful to investigate

† On leave from Institute for Chemical Research, Kyoto University.
‡ Kyoto University.
§ Present address: Institut für Physik, Universität Potsdam, Am Neuen Palais 10, D-14469 Potsdam, Germany.
* To whom correspondence should be addressed: E-mail: neher@rz.uni-potsdam.de.

10.1021/ma000855w CCC: $19.00
Published on Web 10/13/2000

the electromechanical properties of thin polymer films.[18,24−28] The interferometer setup can directly measure the change in film thickness induced by an applied electric field and separate the contributions of electrostriction and piezoelectricity to the field-induced thickness change with the aid of frequency selective (lock-in) detection. The polarization and mechanical compliance of the film are obtained from the electrostrictive and piezoelectric responses, if the dielectric constant is known. We show that the dielectric and ferroelectric properties of the 54 mol % VDF copolymer remarkably depend on layer thickness if the thickness is less than a few hundred nanometers. To elucidate the origin of such layer thickness effects, the layer-thinning effects on the degree of (ferroelectric) crystallinity and the orientation of the ferroelectric crystallites have been investigated by differential scanning calorimetry (DSC) and transmission electron microscopy (TEM), respectively.

Electromechanical Interferometry

The details of the electromechanical interferometry and the setup used in the present study were described elsewhere.[18,24−28] We describe here the outline of the interferometry. The interferometric technique is based on the Nomarski principle.[29,30] As described in Experimental Section, a polymer layer is sandwiched between top and bottom metal electrodes, and two independent and equivalent parallel plate capacitors with such a configuration are constructed on a common glass substrate. Two orthogonally polarized laser beams are reflected at each of the top electrodes of the probe and reference capacitors. When an electric field is applied to only the probe capacitor, a phase shift (ϕ) between the two (probe and reference) beams is generated due to a field-induced thickness change (Δh) as $\phi = 4\pi\Delta h/\lambda$. At the working point of the interferometer, $\phi(\Delta h)$ is proportional to the intensity difference ($A - B$) between two orthogonal polarized beams which are split from the beam recombine after reflection. The modulation in ($A - B$), namely ϕ, is directly analyzed with aid of a lock-in amplifier.

The thickness changes Δh of the parallel plate capacitor induced by an applied electric field (E) can be written as

$$\frac{\Delta h}{h_0} = dE + aE^2 + d'E^3 + a'E^4 + ... \qquad (1)$$

where h_0 is the film thickness without external field. Odd-order terms with coefficients d and d' originate from the inverse-piezoelectric effect (in the following, denoted as the piezoelectric contributions) and are present only for the poled samples. The even-order terms with the coefficients a and a' are due to the electrostrictive effect and present in samples also with a centrosymmetric structure. For paraelectric materials, electrostrictive contributions of the higher-order nonlinear terms such as $a'E^4$ are negligible relative to the contribution aE^2, unless the applied electric field is strong. For ferroelectric materials, the higher-order terms give significant contributions to Δh even under fairly small electric field as shown later and in a previous study.[18]

Under a sinusoidal electric field $E = E_0\cos(\omega t)$, Δh is composed of the sum of $\Delta h(n\omega)$ modulated at certain harmonics of the driving electric field:

$$\frac{\Delta h}{h_0} = \left(\frac{1}{2}aE_0^2 + \frac{3}{8}a'E_0^4 + ...\right) + \left(dE_0 + \frac{3}{4}d'E_0^3 + ...\right)\cos(\omega t) + \left(\frac{1}{2}aE_0^2 + \frac{1}{2}a'E_0^4 + ...\right)\cos(2\omega t) + ... \qquad (2)$$

$\Delta h(\omega)$ and $\Delta h(2\omega)$ originate from piezoelectricity and electrostriction, respectively. Experimentally, $\Delta h(\omega)$ and $\Delta h(2\omega)$ are separately measured by frequency selective (lock-in) detection. The linear coefficients d and a are related to particular physical properties such as plate compliance (k_p), dielectric constant (ϵ), and remanent polarization (P_r) as follows.[18,24−28]

$$d(\omega) = -k_p(\omega)P_r\frac{\epsilon'(\omega_0) + 2}{3} \qquad (3)$$

$$a(2\omega) = -\frac{\epsilon_0 k_p(2\omega)}{2}\left[\epsilon'(\omega) + \frac{(\epsilon'(\omega) + 2)(\epsilon'(\omega) - 1)}{3}\right] \qquad (4)$$

where $\epsilon'(\omega)$ and $\epsilon'(\omega_0)$ are the real part of linear dielectric constants at the driving frequency (ω) and optical frequency (ω_0), respectively. The plate compliance k_p is related to the bulk compressibility k_b as $k_b = 3k_p(1 - \nu)/(1 + \nu)$ with Poisson's ratio ν. This relation is based on the employed sample geometry which does not allow appreciable horizontal expansion in the film plane by vertical compression:[25] The film is fixed in the plane onto the substrate, and the film thickness is about a factor of at least 1000 smaller than the lateral extension.

In deriving eqs 3 and 4, the polarization in the plate capacitor is replaced by an equivalent charge density, and the following Clausius−Mossotti relation is employed for $\partial\epsilon/\partial h$:

$$\frac{\partial\epsilon}{\partial h} = -\frac{(\epsilon - 1)(\epsilon + 2)}{3h} \qquad (5)$$

Experimental Section

Sample Preparation. The P(VDF-TrFE) polymer with 54 mol % VDF content was kindly supplied by Daikin Kogyo Co. No information on the molecular weight of the material is yet available. The samples for dielectric and electromechanical spectroscopy were prepared as follows: The copolymer was spin-coated on the surface of a glass substrate on which three thin Al strips of 35 nm thickness were previously evaporated as bottom electrodes. Films with different thickness were prepared from 2-butanone solutions with different polymer concentrations (ranging from 20 to 84 mg/mL). The spin-coated films were annealed at 140 °C for 1 h. A top Al strip electrode of 60 nm thickness was deposited with an orientation perpendicular to that of the bottom strips. Thus, a sandwich-type structure with three independent capacitors (one of which is for reserve) were constructed. The film thickness was measured by a Tencor α-step profiler.

Poling of the films was performed at room temperature by applying an ac electric field of 100−230 MV/m and 0.01 Hz for 10 cycles. For each sample piezoelectric measurement were performed to make sure that the achieved polarization was saturated against applied poling field.

Electromechanical Interferometry. The modulation (detection) frequency was 5000 Hz in both the electrostriction and piezoelectric measurements. The half of the modulation frequency of 5000 Hz was used as the driving frequency (ω) for electrostriction measurements, because electrostriction modulates the film thickness at double the frequency of the applied field (2ω), and the dynamic compliance is generally frequency-dependent.

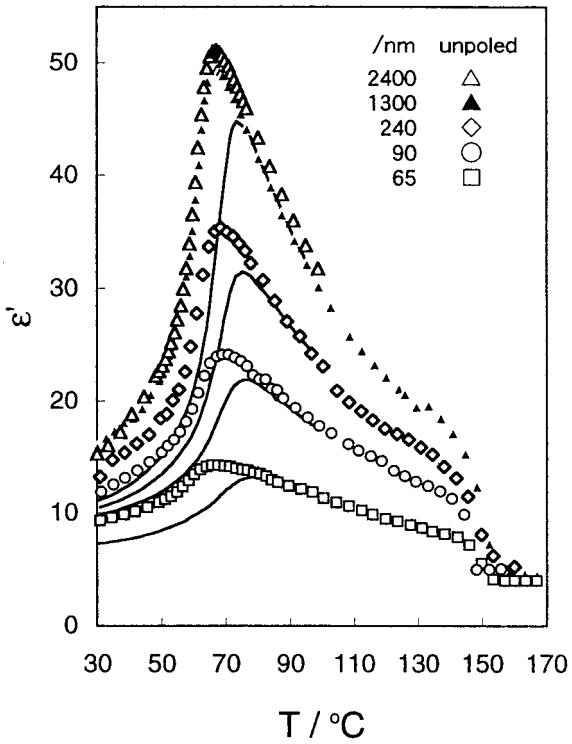

Figure 1. Temperature dependence of the real part of the linear dielectric constant ϵ' for unpoled and poled copolymer layers with different thicknesses. The solid lines represent the data of the poled samples.

Dielectric Spectroscopy. Linear dielectric measurements were performed at 2500 Hz just prior to the electromechanical measurements at each temperature using a home-built current/voltage amplifier in combination with a lock-in amplifier Stanford Research Systems SR830.

Differential Scanning Calorimetry (DSC). A copolymer film spin-coated on an Al foil substrate was immersed in an aqueous solution of sodium hydroxide which dissolves the Al foil but does not damage the copolymer film. The resulting copolymer films of ca. 10 mg without the substrate were used for DSC measurements. The DSC measurements were performed by a Rigaku DSC8230B instrument with a heating rate of 10 °C/min.

Transmission Electron Microscopy (TEM). Morphological studies of the film surface were made with a transmission electron microscope JEOL JEM-100U operated at an accelarating voltage of 80 kV using the surface replica method. A 65 nm thick film removed from a glass substrate was used for electron diffraction (ED) experiments. The ED experiments were made at room temperature using a transmission electron microscope JEOL JEM-200CS operated at 200 kV equipped with a rotation-tilt specimen holder (JEOL EM-SRH10).

Results and Discussion

Dielectric Constant. Figure 1 shows the temperature (T) dependence of the real part of the linear dielectric constant ϵ' for the unpoled and poled films with different film thicknesses (h). All $\epsilon'-T$ curves have a definite maximum corresponding to the ferroelectric-to-paraelectric phase transition. The decrease in ϵ' around T = 150 °C is due to the melting of the paraelectric crystal, which will be shown later in the DSC results. No appreciable difference is observed between the 1300 and 2400 nm thick films, while for the films with thickness $h \leq 240$ nm ϵ' is fairly smaller in the region $T < 150$ °C, compared to the thicker layers. In addition, ϵ' significantly decreases with a decrease in h for $h \leq 240$ nm. Also, ϵ' is smaller for the poled samples, and the maxima are located at a higher temperature, relative to the corresponding unpoled samples. These differences are attributed to a higher perfection of the crystal structure after poling.[31]

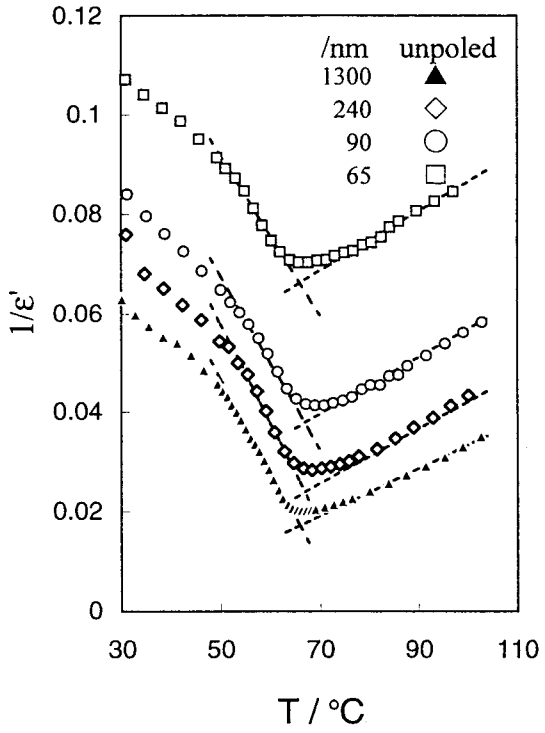

Figure 2. Curie plots for unpoled copolymer layers with different thicknesses. The phase transition temperature T_c for each sample was estimated from the intersection of the two straight dashed lines.

The ferroelectric-to-paraelectric phase transition of the P(VDF-TrFE) with more than 50 mol % VDF content is considered to be of thermodynamical first order on the basis of a finite thermal hysteresis in the dielectric behavior.[7,31] A classical theory predicts the T dependence of the reciprocal permittivity $1/\chi$ near a first-order phase transition as[32]

$$1/\chi = (T_c - T)/C_1 + \alpha_0 \quad (T < T_c) \tag{6a}$$

$$= (T - T_c)/C_2 + \alpha_0 \quad (T > T_c) \tag{6b}$$

where C_1, C_2, and T_c are the Curie constants and the phase transition temperature (the Curie temperature), respectively, and α_0 is a constant. In the case of second-order phase transition, α_0 is zero, corresponding to a divergence of χ at T_c, and then eq 6 coincides with the Curie−Weiss law.

The Curie plots ($1/\epsilon'$ vs T) for the unpoled films with different thicknesses are presented in Figure 2. The inverse of ϵ', $1/\epsilon'$, varies linearly with T in the vicinity of the minimum of $1/\epsilon'$ for each sample. T_c and α_0 were estimated from the intersection of the two straight lines of the plots of $1/\epsilon'$ vs T.[3] The values of T_c, C_1, C_2, and α_0 for the unpoled and poled samples are tabulated in Table 1. No significant dependence of T_c or the Curie constants on h is found for both the unpoled and poled samples. This observation is in agreement with the findings on ultrathin ferroelectric LB films[19−22] as discussed above. In the latter case, the Curie temperature of the ultrathin layers (of thicknesses between 1 and 15 nm) was nearly equal to the bulk value, and

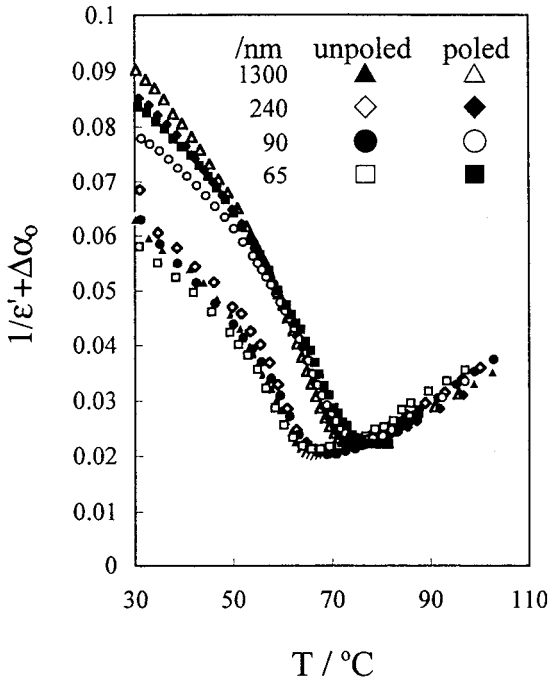

Figure 3. Superposition of the Curie plots for unpoled copolymer layers with different thicknesses by a vertical shift by $\Delta\alpha_0$, with $\Delta\alpha_0 = \alpha_0(h{=}1300\text{ nm}) - \alpha_0(h)$.

Table 1. Values of T_c, C_1, C_2, and α_0 for Unpoled and Poled P(VDF-TrFE) Films

film thickness (nm)	T_c (°C)	$C_1 \times 10^{-2}$ (K)	$C_2 \times 10^{-3}$ (K)	$\alpha_0 \times 10^{-2}$
1300 (unpoled)	66	5.40	2.10	1.71
240	67	4.98	1.81	2.38
90	67	5.70	1.73	3.71
65	66	6.23	1.68	6.48
1300 (poled)	72	4.18	2.05	1.86
240	73	4.43	2.16	2.86
90	74	4.91	1.68	4.14
65	74	4.64	1.94	7.43

there was no evidence for a critical minimum thickness below which the ferroelectricity vanishes. In fact, a second transition was observed at approximately 20 °C and attributed to ferroelectric ordering in the topmost layer of the LB.[19,33] In our experiments on spin-coated layers we find no evidence for a second transition in the ferroelectric phase, which might be due to the rather large minimum thickness of our layers. However, α_0 increases with decreasing h corresponding to an increase in the minimum of $1/\epsilon'$. Actually, all the $1/\epsilon'$ vs T curves for different h are satisfactorily superposed by a vertical shift $\Delta\alpha_0$, where $\Delta\alpha_0$ is the difference in α_0 to a reference sample. Figure 3 shows the result of the superposition for the unpoled and poled samples using $h = 1300$ nm as a reference. The successful superposition implies that the layer thinning reduces the dielectric constant of the system but does not significantly influence the essential nature of the phase transition. The results in Figures 2 and 3 suggest that the observed layer-thinning effect on the dielectric constant could be interpreted by the contribution of a nonferroelectric thin surface near layer: In this case, the layer may be considered as a serial capacitor composed of the thin nonferroelectric layer of thickness h_s with a lower dielectric constant ϵ_s and the bulklike ferroelectric layer of thickness $h_B = h - h_s$ with the dielectric constant ϵ_B. Since the total electric capacitance C_t is expressed as $1/C_t = 1/C_s + 1/C_B$ where C_s and C_B is the capacitance

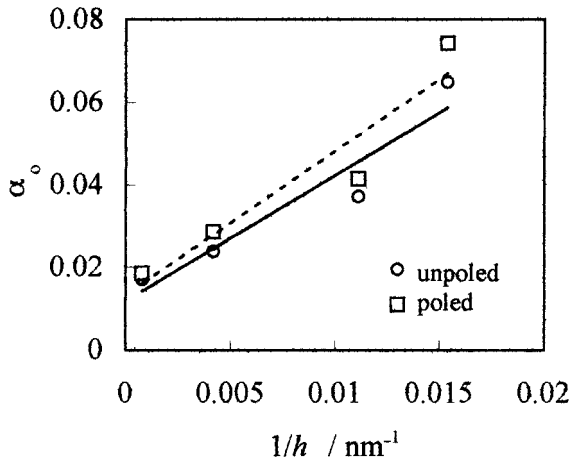

Figure 4. Plot of α_0 against the inverse of the layer thickness for unpoled and poled samples. The solid and dashed lines represent the results of linear regression for unpoled and poled samples. According to eq 7, the slope and intersection at $1/h = 0$ yield the values of $(1/\epsilon_S - 1/\epsilon_B)h_S$ and $1/\epsilon_B$, respectively: $1/\epsilon_B = 1.18 \times 10^{-2}$, 1.34×10^{-2}; $(1/\epsilon_S - 1/\epsilon_B)h_S = 3.05$ and 3.48 for unpoled and poled samples, respectively.

of the surface and bulk layer, respectively, the total dielectric constant ϵ is written as

$$\frac{h}{\epsilon} = \frac{h_s}{\epsilon_s} + \frac{h - h_s}{\epsilon_B} \tag{7}$$

Figure 4 shows the plots of α_0 (corresponding to the inverse of maximum of ϵ') versus the inverse of film-thickness for the unpoled and poled samples. On the basis of eq 7, the gradient and intersection at $1/h = 0$ produce $(1/\epsilon_s - 1/\epsilon_B)h_s = 3.05$, 3.48 and $1/\epsilon_B = 1.18 \times 10^{-2}$, 1.34×10^{-2} for the unpoled and poled samples, respectively. If $\epsilon'_s \approx 4$ is assumed in the amorphous state, this gives $h_s \approx 12$ and 14 nm for the unpoled and poled samples. Thus, the decrease in ϵ' with layer thinning might be explained as a result of the increase in the contribution of the amorphous-like surface near layer with a lower dielectric constant to the overall dielectric signal. A contribution of a thin Al_2O_3 layer at the interface of the Al electrodes to the polymer layer cannot be fully excluded, but in general, those interfacial Al_2O_3 layers are very thin (less than 1 nm). The effects of the thin nonferroelectric surface near layer will also be discussed later together with the calorimetric results of the thin films.

Electrostriction. Figure 5 shows the plots of the field-induced thickness change due to electrostriction (Δh_{ES}) against the square of the applied electric field (E_0^2) for the unpoled 240 nm thick film in the paraelectric phase ($T > T_c$). Δh_{ES} varies linearly with E_0^2 in the E_0 range examined here, and the linear coefficient a for electrostriction was estimated from the slope of the straight line.

The plots of Δh_{ES} vs E_0^2 in the ferroelectric phase ($T < T_c$) of the unpoled 240 nm thick film are illustrated in Figure 6. The E_0^2 dependence of Δh_{ES} is remarkably nonlinear, and a considerable nonlinearity is observed even at $T = 64.1$ °C close to T_c. For amplitudes E_0 lower than ca. 70 MV/m, Δh_{ES} varies linearly with E_0^2, which allows to determine the linear coefficient a by extrapolation toward zero field. Similar nonlinear electrostriction effects in the ferroelectric phase were first reported in our previous paper[18] for an unpoled 1300 nm thick film of the same copolymer. It was shown that the

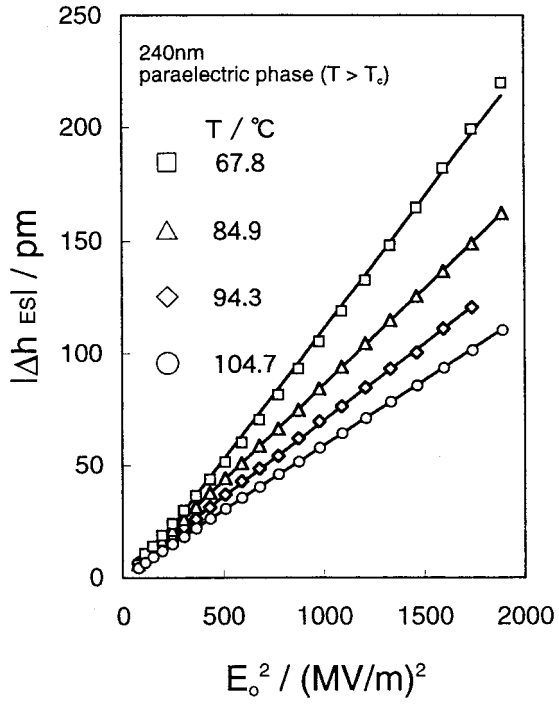

Figure 5. Dependence of the field-induced thickness change due to electrostriction Δh_{ES} on the square of the applied electric field E_0^2 for an unpoled 240 nm thick film in the paraelectric phase.

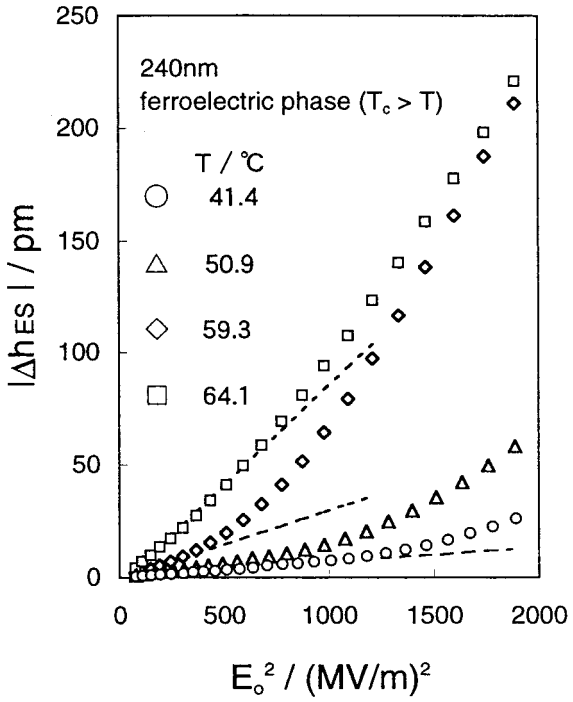

Figure 6. Dependence of the field-induced thickness change due to electrostriction Δh_{ES} on the square of the applied electric field E_0^2 for the unpoled 240 nm thick film in the ferroelectric phase. Dashed lines represent the linear extrapolations toward zero field.

experimental nonlinear electrostriction was much larger than a theoretical prediction taking into account the nonlinear third-order dielectric constant, except in the vicinity of T_c.[18] An interaction between and/or within the ferroelectric domains in the polydomain structure, which is not considered in the theory, was expected to be a major origin of the nonlinear electrostriction.[18]

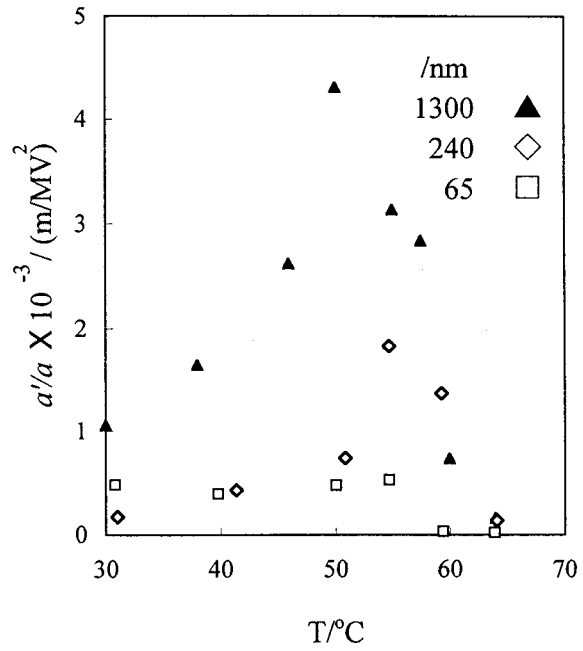

Figure 7. Ratio a'/a for unpoled samples with different layer thicknesses as a function of temperature.

To discuss the effects of temperature and layer thickness on the nonlinear electrostriction, we used the coefficient ratio a'/a as a measure of degree of nonlinearity, obtained by fitting the equation $\Delta h_{ES}/h_0 = (aE_0^2 + a'E_0^4)/2$ to the experimental data. The T dependence of a'/a for the 1300, 240, and 65 nm thick films is presented in Figure 7. In the entire T range the degree of nonlinearity is smaller for the 240 and 65 nm thick films compared to the 1300 nm thick film. The ratio a'/a has a maximum at $T = 50-55$ °C for the 1300 and 240 nm thick films, while a'/a for the 65 nm thick film does not have a definite maximum and becomes close to zero near $T = 60$ °C, fairly below T_c. Such layer thickness effects on nonlinear electrostriction suggest that the ferroelectric character of the films is weakened by thinning the copolymer layer.

It should be noted that a quantitative measurement of the nonlinear electrostriction for the poled samples was not possible, because the high electric fields necessary to reach the nonlinear region disturbed (reduced) the original polarization in the samples. This point was discussed in our previous paper.[18] The linear coefficient a for the poled samples was evaluated by linear regression using the data in a low-E_0 region where the original polarization is not disturbed.

Figure 8 shows the T dependence of the linear electrostriction coefficient a for the samples with different thicknesses. The $a-T$ curves have a maximum around T_c, and the maximum value decreases with a decrease in h. The h dependence of the $a-T$ curves is qualitatively similar to that of the $\epsilon'-T$ curves. As is seen in eq 4, a is a product of the plate compliance and an increasing function of ϵ'. The similarity of the $\epsilon'(T)$ and $a(T)$ curves suggests that the T dependence of a is mainly governed by the T dependence of ϵ'.

Plate Compliance. Figure 9 shows the values of k_p as obtained using eq 4 with experimental data of ϵ' and a as a function of T for the unpoled samples. It is common to all samples that k_p increases in a stepwise fashion with T. The results for the poled samples are essentially similar to those for the unpoled ones except

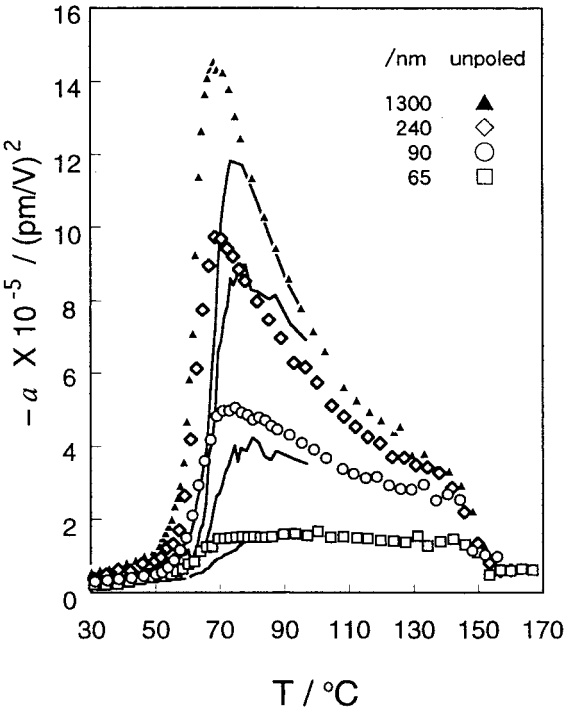

Figure 8. Temperature dependence of the linear electrostriction coefficient $-a$ for unpoled samples with different layer thicknesses. Solid lines represent the data for the poled samples.

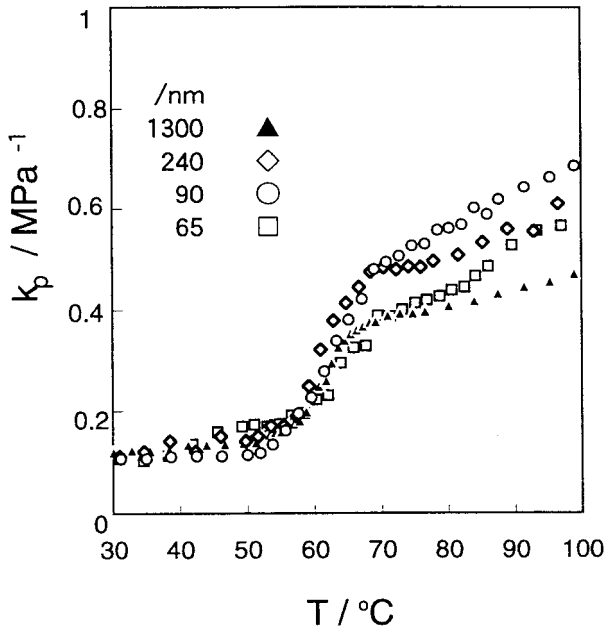

Figure 9. Temperature dependence of the plate compliance k_p for unpoled samples with different layer thicknesses.

for the location of T_c. The data for the poled samples are not shown here. As can be seen in the figure, k_p calculated from electrostriction is almost independent of layer thickness. This suggests that the applied electric field is not reduced inside the layer due to a hypothetical thick isolation layer such as Al_2O_3. The T dependences of the Young's modulus[9] and bulk modulus[34] of thick samples of ca. 52 mol % VDF copolymer were reported, but their results in the vicinity of T_c were much different: The Young's modulus vs T curve only showed an inflection around T_c,[9] while the bulk modulus vs T curve exhibited a conspicuous minimum at T_c.[34] k_p is

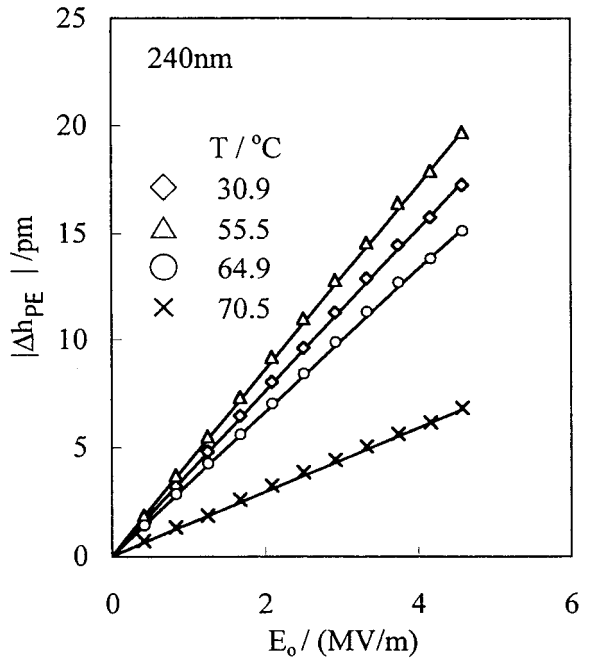

Figure 10. Dependence of the field-induced thickness change due to piezoelectricity Δh_{PE} on the applied electric field amplitude E_0 for a poled 240 nm thick film.

related to both Young's modulus and bulk modulus by an equation from classical elasticity theory. However, the direct comparison of the present and earlier studies is rather questionable because they strongly defer in the pretreatments of samples such as annealing and drawing. A systematic study on different elastic moduli of the same sample will be necessary in order to elucidate the elastic behavior in the vicinity of T_c.

Piezoelectricity. Figure 10 shows the field-induced thickness change due to piezoelectricity (Δh_{PE}) as a function of applied electric field amplitude E_0 for the poled 240 nm thick film. The electric field amplitudes were small enough not to disturb the original polarization. In this case, Δh_{PE} increases linearly with E_0, and the linear piezoelectric coefficient d was evaluated by linear regression.

Figure 11 shows the T dependence of d for the poled samples. For all samples, d slightly increases with an increase in T in the region of $T < 50$ °C, while it decreases in the range of $T > 55$ °C and becomes zero around T_c. No significant differences in the $d-T$ curves are observed for the films of $h \geq 90$ nm, while the absolute values of d in the region of $T < 65$ °C are significantly smaller for the 65 nm thick sample. Because k_p is not significantly dependent on h in the region of $T < T_c$, as shown in Figure 9, the smaller d for the 65 nm thick film mainly originates from a smaller P_r.

Remanent Polarization. The remanent polarization P_r was calculated by eq 3 with values of d and k_p obtained from electromechanical measurement with low field amplitudes. $\epsilon' = 4.0$ at 200 MHz reported for a poled P(VDF-TrFE) film[36] was used as $\epsilon'(\omega_0)$ in eq 3. Figure 12 shows the calculated P_r for the poled films with different thicknesses as a function of T. The absolute values of P_r and its T dependence for the films of $h \geq 90$ nm are almost the same, while the 65 nm thick film shows a considerably smaller P_r. As stated in the Experimental Section, P_r for each sample was experimentally checked to be maximum (saturated) against

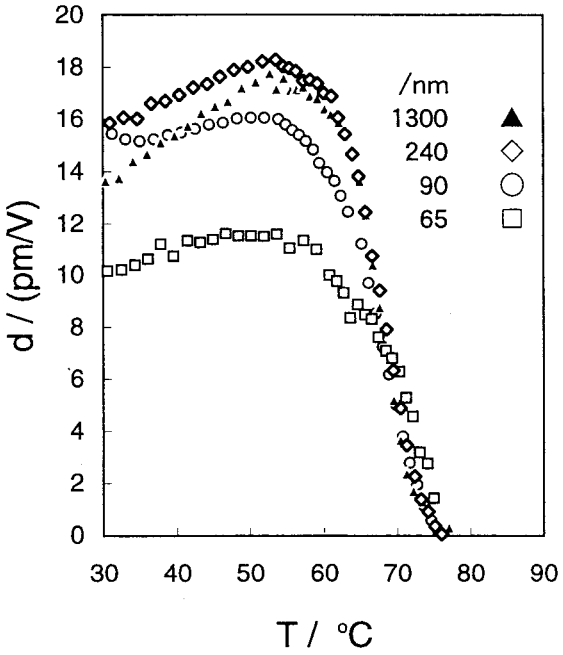

Figure 11. Temperature dependence of the linear piezoelectric coefficient *d* for poled samples with different layer thicknesses.

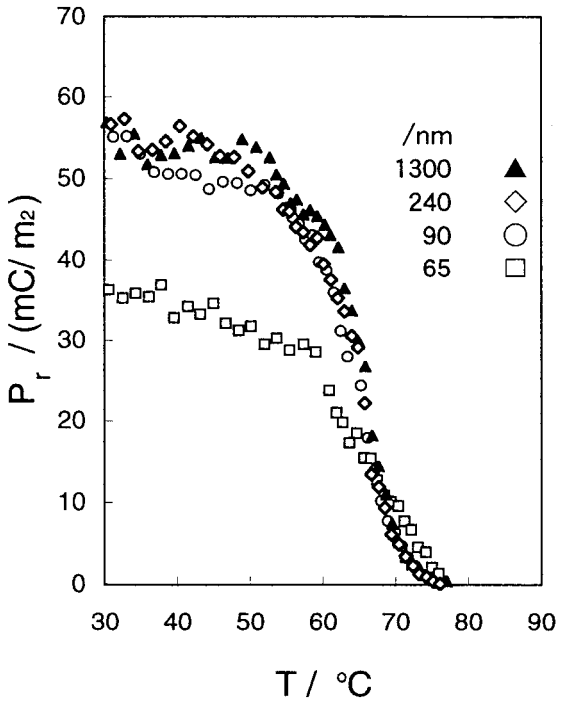

Figure 12. Temperature dependence of the remanent polarization P_r for poled samples with different layer thicknesses.

the poling field. $P_r = 55-57$ mC/m^2 at $T \approx 30$ °C for the films with $h \geq 90$ nm is close to the reported values 55 and 63 mC/m^2 for 45[37] and 20 μm thick[38] films, respectively, of a P(VDF-TrFE) with almost the same VDF composition (52 mol %). The two reported values were obtained by different experimental techniques such as thermally stimulated current[37] and electric displacement (D)−E hysteresis methods.[38] The fairly good agreement between the reported values and P_r for the films of $h \geq 90$ nm suggests that the polarization achieved in the copolymer layers is as large as that for the bulk samples, provided that the film thickness exceeds ca. 100 nm.

The remanent polarization gradually decreases with increasing T in the range of 55 °C < T < T_c. The gradual reduction of P_r, instead of sharp drop of P_r at $T = T_c$, can be understood in terms of the coexistence of the paraelectric crystalline phase with the ferroelectric crystalline phase over a finite temperature range. Some studies[7,35] reported that the coexistence region extends from T_c down to ca. T_c −10 K for 60 mol % VDF copolymer. In the coexistence region, with increasing T, the volume fraction of the ferroelectric crystalline phase decreases, while a concurrent increase of the volume fraction of the paraelectric phase is observed.[7] Such type of crystalline transformation in the coexistence region will gradually reduce the remanent polarization as well as the piezoelectric response (Figure 10) in the range of 55 °C < T < T_c.

The significantly smaller P_r for the 65 nm thick film is in contrast to the results by Kimura et al.[23] for a 60 nm thick film of P(VDF-TrFE) with 75 mol % VDF. These authors demonstrated that the saturated polarization for the 60 nm thick film is comparable to that for thicker films, though the thinner the film thickness, the larger is the minimum poling field necessary for saturation of polarization. Poling field amplitudes as large as 200 MV/m were found to be necessary for the polarization saturation in the 60 nm thick film. The maximum poling field in the present study (230 MV/m) exceeded this value, and saturation of polarization was observed. The difference in the polarization behavior of the ca. 60 nm thick film in their and our studies might be due to the difference in VDF. As reported elsewhere,[39] the crystallinity as well as P_r of P(VDF-TrFE) increases with an increase in VDF content unless the VDF contents exceed 80 mol %. In the case of the P(VDF-TrFE) with 75 mol % VDF content, the ferroelectric crystallinity will still be high enough to achieve large polarization even in the 60 nm thick film, though it was also observed that the crystalline grains in the 60 nm thick film are smaller than that in thicker films.[23] On the other hand, for the P(VDF-TrFE) with 54 mol % VDF content, the crystallinity will be more readily influenced by thinning the copolymer layer due to the relatively low crystallizability of the copolymer itself. The effect of layer thinning on crystallinity will be shown in the DSC results. Bune et al.[22,40] reported that the ultrathin LB film composed of 30 monolayers of 70 mol % VDF copolymer has a polarization comparable to that of the thicker spin-coated films. The high ability of polarization of the LB film originates from the high crystallinity and crystal orientation achieved by LB monolayer transfer technique.[22,40]

DSC. Figure 13 shows the DSC thermograms of the unpoled films with different thicknesses. The two endothermic peaks around $T = 65$ °C and $T = 155$ °C are assigned to the ferroelectric-to-paraelectric phase transition and the crystalline melting, respectively. As the film thickness becomes smaller, the peak related to the phase transition becomes broader, and the peak area for the crystalline melting becomes smaller. The enthalpy of fusion (ΔH_m) and the crystalline melting temperature (T_m) for each sample are summarized in Table 2. ΔH_m decreases with decreasing film thickness, indicating that the degree of crystallinity is smaller in thin samples. In particular, the crystallinity of the 65 nm thick film is much lower than that of the 90 nm thick layer. It has often been observed that T_m decreases with reduction in crystallite size,[41] but in the present study

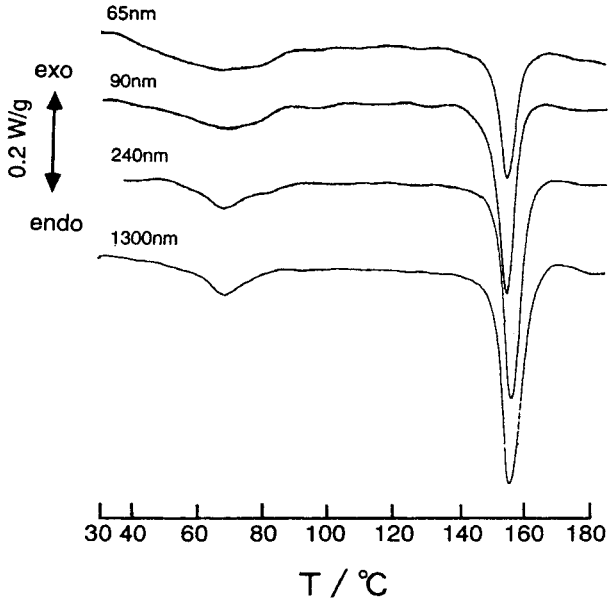

Figure 13. DSC thermograms of unpoled samples with different layer thicknesses. The two endothermic peaks around $T = 65$ °C and $T = 155$ °C are assigned to the ferroelectric-to-paraelectric phase transition and the crystalline melting, respectively.

Table 2. Crystalline Melting Temperatures (T_m) and Heats of Fusion (ΔH_m) of P(VDF-TrFE) Films

film thickness (nm)	T_m (°C)	ΔH_m (J/g)
1300	156.3	27.9
240	156.1	24.6
90	154.6	22.1
65	155.0	15.6

no significant effect of h on T_m was observed. However, the definite reduction in ΔH_m by layer thinning should be interpreted as a result of decrease in degree of crystallinity.

As in the case of the layer-thinning effect on the dielectric constant, the degree of crystallinity with decreasing h might be explained by the presence of a thin surface near layer of thickness h_S with a lower melting enthalpy ΔH_S (or a lower degree of crystallinity) and a bulklike layer with the enthalpy ΔH_B. The total melting enthalpy ΔH_m may be written as a sum of each contribution in the following:

$$h\Delta H_m = h_S\Delta H_S + (h - h_S)\Delta H_B \qquad (8)$$

Figure 14 illustrates the plots of $\Delta H_m(h)$ against the inverse of layer thickness. According to eq 8, the slope and intersection at $1/h = 0$ of the plots yield the values of $(\Delta H_S - \Delta H_B)h_S$ and ΔH_B, respectively: $\Delta H_B = 28.5$ J g^{-1}; $(\Delta H_S - \Delta H_B)h_S = -757$ J g^{-1} nm^{-1}. If one assumes $\Delta H_S = 0$, then h_S is ca. 27 nm, which is comparable in magnitude but slightly larger than $h_s = 12$ nm evaluated from $\epsilon'(h)$ using eq 7. The appreciable difference in the two values of h_s derived from the thickness dependence of ϵ' and ΔH_m is not fully understood but might be attributed to the preferential orientation of the crystals as discussed in the next section. Also, the evaluation of the data based on eqs 7 and 8 is quite critical due to the small number of data points. The good linearity and the reasonable values obtained from the linear regression in both the plots, however, suggest that both the layer-thinning effects on ϵ' and ΔH_m can be consistently explained when assuming a

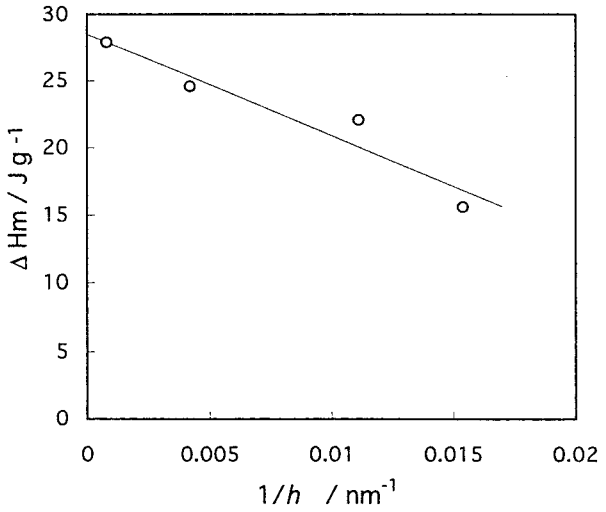

Figure 14. Plots of $\Delta H_m(h)$ against the inverse of layer thickness. According to eq 8, the slope and intersection at $1/h = 0$ of the plots yield the values of $(\Delta H_S - \Delta H_B)h_S$ and ΔH_B, respectively: $\Delta H_B = 28.5$ J g^{-1}; $(\Delta H_S - \Delta H_B)h_S = -757$ J g^{-1} nm^{-1}.

thin amorphous-like surface near layer: The reduction in ϵ' and ΔH_m with layer thinning can be interpreted in terms of the increase in the relative contribution of the thin amorphous-like surface near layer with a lower melting enthalpy as well as a lower dielectric constant to the overall layer. We like to point out that this observation might be a direct consequence of the preparation by spin-coating. As outlined above, ultrathin LB assemblies prepared by layerwise deposition did not exhibit a significant dependence of the properties with film thickness.[19−22] It is thus meaningful to conclude that the layer-thinning effects observed here are caused by changes in the morphology, crystallinity, and chain orientation in the spin-coated layers and not a direct consequence of reduced dimensionality.

It should be noted that the ratio of ΔH_m of the 65 nm thick film to the 1300 nm thick one (∼0.56) is slightly smaller than but close to the ratio of P_r at room temperature (∼0.64). These DSC results suggest that the h dependence of the dielectric and electrostrictive behaviors mainly originates from a decrease of crystallinity due to layer thinning and that the smaller polarization in the 65 nm thick film is closely related to the lower content of ferroelectric crystal.

TEM. A specific orientation of the (ferroelectric) crystallites in the thin copolymer layer, if any, can further influence the dielectric and electromechanical properties. Figure 15 shows TEM photographs for surface replicas of the copolymer films with $h = 1300$ (Figure 15a), 240 (Figure 15b), and 65 nm (Figure 15c). It can be seen that the surface becomes smoother as the film thickness decreases. The variation of the surface roughness against h is qualitatively similar to the h dependence of degree of crystallinity revealed by DSC. The surface roughness is likely to be dominated by the size of crystalline grains. However, we cannot rule out the possibility of surface smoothing for thinner layers due to some preferred orientation of the crystalline grains.

Figure 16 shows the ED patterns from the unpoled 65 nm thick film untilted (Figure 16a) and tilted by ca. 30° and ca. 60° around the axis parallel to the equator (Figure 16, b and c, respectively). The ED experiment was not carried out for the poled 65 nm thick film due

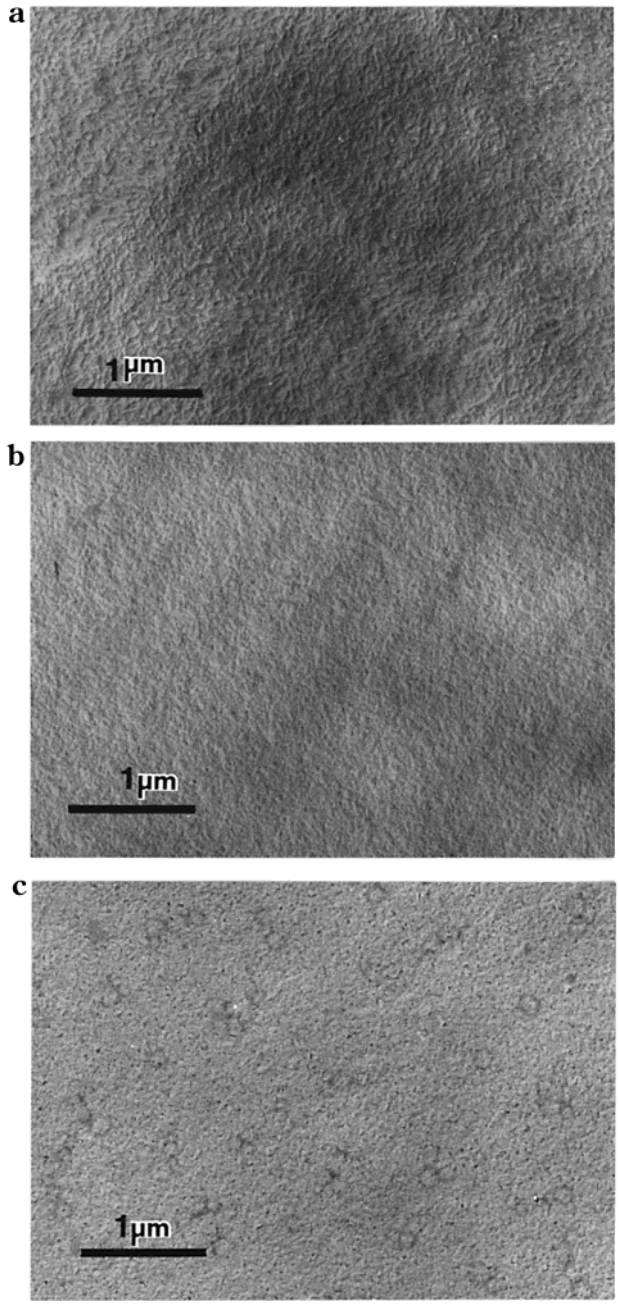

Figure 15. TEM photographs for the surface replicas of the unpoled samples with different layer-thicknesses: (a) 1300 nm, (b) 240 nm, (c) 65 nm.

to the difficulties to remove the electrodes (which are required for poling and which are too thick to transmit the electron beam) without giving serious damage for TEM observation. In Figure 16a, all the reflection rings have uniform intensity distribution along the Debye−Scherrer circle, which shows that the crystallites in the thin layer have random orientation in the plane parallel to the film surface (or substrate). These rings seem to correspond to the reflections from the (110) + (200), (001), (220) + (400), and (002) planes, as indicated in the figure. These assignments were made on the basis of the reported lattice spacings for *the cooled phase* of the 55 mol % VDF copolymer.[41] Tashiro et al.[41] reported that the ferroelectric crystal of the 55 mol % VDF copolymer has essentially the same structure as the so-called β-phase crystal of PVDF (all-trans structure), but strictly speaking, the ferroelectric crystalline structure

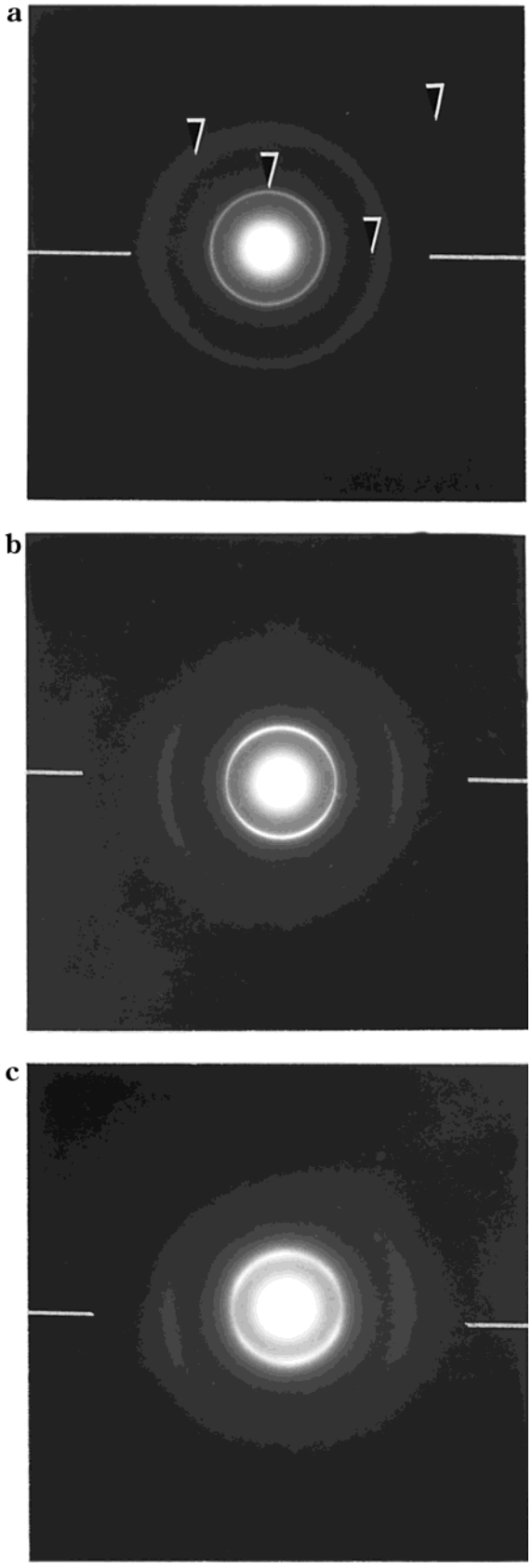

Figure 16. ED patterns from an unpoled 65 nm thick film for normal incidence (a) and tilted by ca. 30° (b) and ca. 60° (c) around the axis parallel to the equator. The rings are assigned to the reflections from (200) + (110) (innermost), (001), (400) + (220), and (002) lattice planes in order of inner location, which is in correspondence to the assignment of the lattice planes for the cooled phase.

is classified into two types depending on thermal history: a *low-temperature phase* for as-cast samples and a *cooled phase* for samples cooled after annealing above T_c. It was observed that the intensity of the 001 reflection was fairly stronger than that of 002 in the low-temperature phase, while the 001 reflection is rather diffuse and the intensities of the 001 and 002 reflections are comparable in cooled phase, although both phases have almost the same lattice spacings of the crystalline structures.[41,42] On the basis of the diffuse and weak reflection of 001 in Figure 16a, the ferroelectric crystalline structure in the 65 nm thick film is assigned to the cooled phase. This assignment accords with the simple expectation from the thermal history of the sample (annealed at 140 °C). It is important to mention that Lovinger et al.[44,45] proposed a different structure model, a mixture of disordered trans-planar and 3/1-helical phases, for the ferroelectric crystal of 52 mol % VDF copolymer. However, we prefer the cooled phase model by Tashiro et al. as the reference because it provides more information about the unit cell parameters and the structure factors necessary for the assignments of the reflections. Furthermore, the cooled phase model was reported to be consistent with the results of infrared spectroscopy.[42]

When the specimen is tilted around a certain axis (around the equator in Figure 16), each ring becomes arc-shaped: With increasing tilting angle, the intensity in the meridional part of the innermost ring becomes stronger, while the intensity in its equatorial part is unchanged. The meridional parts of the 400 + 220 and 002 rings disappear first, and its remaining arcs on the equator become shorter. The 001 and 002 rings are invisible at tilting angles over 30° and 60°, respectively. These results reveal that there is a specific orientation of the crystallites in the plane perpendicular to film surface (or substrate). Unfortunately, it was difficult to quantitatively characterize the orientation of the crystallites, which is due to the low degree of crystallinity of the specimen and the small numbers of visible reflections. For example, no additional reflections appeared when the specimen was tilted. On the basis of the limited information, it is tentatively speculated that the crystallites are preferentially oriented with their (010) plane being parallel to the film surface (or substrate), taking into account the fact that the meridional part of the 110 reflection becomes more intense with increasing tilting angle. Though the 110 and 200 reflections are almost overlapped in the innermost ring, it will be plausible to attribute the major contribution of the intensity increase by tilting to the 110 reflection, because the reported structure factor of the 110 reflection is definitely larger than that of the 200 reflection in the cooled phase.[41] The speculated model implies that the chain axis of the all-trans crystalline structure is preferentially aligned parallel to the substrate. However, it is worth noting that the crystal structure of the cooled phase is constructed by bent trans segments including skew linkages (what they call the 60° domain structure).[41] Consequently, the directions of the CF_2 dipoles in the cooled phase are not globally unique (but locally unique) in the molecular chains. The lack of any spontaneous piezoelectricity (polarization) in the unpoled samples directly proves the absence of a global orientation of the CF_2 dipoles in a unique direction perpendicular to the film surface. It should also be noticed that, in principle, the ED pattern analysis for the types of samples used here cannot distinguish between certain chain configuration and its mirror image having the CF_2 dipoles in the opposite direction.

As described previously, the smaller polarization in the 65 nm thick layer is explained by the reduction of the overall crystallinity as suggested by the thickness-dependent melt enthalpy (ΔH_m); however, note that the analysis of the h dependence of ϵ' and ΔH_m for the unpoled samples yields considerably different values of h_s (12 and 27 nm, respectively). This difference can be attributed to the much larger sensitivity of the dielectric constant to the crystalline alignment in comparison with the heat of fusion. For example, the preferential crystalline orientation in the thin layer might also alter the dielectric constant of the crystalline phase with decreasing thickness. The h dependence of the dielectric and electromechanical properties is thus interpreted as a result as a combined effect of the reduction in crystallinity and the enhancement in the specific crystalline orientation due to layer thinning.

Summary

Ferroelectricity and the ferroelectric-to-paraelectric phase transition in a thin layer of P(VDF/TrFE) with layer thicknesses (h) ranging from 1300 nm down to 65 nm have been studied with respect to dielectric and electromechanical properties. Electrostriction and inverse-piezoelectric effects of thin copolymer layers were investigated utilizing an electromechanical interferometer. In the region of h less than a few hundred nanometers, pronounced effects of layer thinning on the dielectric and electrostrictive behaviors are observed. The dielectric constant and the linear electrostrictive coefficient decrease with reduction in h. The electrostriction in the ferroelectric phase shows a nonlinear dependence on the square of the applied electric field, and the degree of nonlinearity decreases as the layers becomes thinner. On the other hand, no significant effects of layer thinning on the phase transition temperature or the Curie constants are observed. The remanent polarization (P_r) in the thin copolymer layers as induced by poling was evaluated from the data of the electrostrictive and inverse-piezoelectric effects. A prominent layer-thinning effect on P_r is recognized for the 65 nm thick film. P_r in the 65 nm thick film (40 mC/m^2) is considerably smaller than P_r in the thicker films (ca. 55 mC/m^2). DSC measurements reveal that the degree of crystallinity (the fraction of the ferroelectric crystal) decreases with the decrease in h, and especially, the crystallinity in the 65 nm thick film is rather small. The ratio of the degrees of crystallinity of the 1300 and 65 nm thick films is close to the ratio of the corresponding P_r's. Both the layer thickness dependence of the overall dielectric constant and crystallinity can be consistently interpreted when assuming the presence of an amorphous-like surface near layer. The reductions of the overall dielectric constant and crystallinity by layer thinning might be explained by the increase in the contribution of a thin surface near layer of a lower crystallinity as well as a lower dielectric constant. The analysis of the thickness dependence of ϵ' and ΔH_m assuming the presence of a (nonferroelectric or amorphous) thin surface near layer yielded a layer thickness of 12 and 27 nm for the unpoled samples, respectively. TEM observations for the 65 nm thick film show that the chain axis of the all-trans structure of the ferroelectric crystallites appears to have a preferred orienta-

tion parallel to the film surface (or substrate). The appreciable difference in the values of the surface near layer thickness evaluated from the h dependence of ϵ' and ΔH_m might be attributable to the preferential orientation of the crystals in the thin layer, which is more decisive for ϵ'. These results imply that the layer thickness dependence of dielectric and electromechanical properties is a result of the combination of the reduction in crystallinity and the enhancement in crystalline orientation due to layer thinning.

Acknowledgment. We acknowledge support by Prof. G. Wegner (MPI, Mainz). The stay of K.U. at the MPI in Mainz was financed by a fellowship of the Max-Planck Society. We are indebted to Mr. G. Glasser (MPI, Mainz) for technical support with the electromechanical interferometer, to Mr. M. Ohara (Kyoto University) for TEM observation, and to Mr. M. Fujita (Kyoto University) for the interpretation of TEM results. We thank Daikin Kogyo Co. for providing the copolymer sample.

References and Notes

(1) Yamada, T.; Ueda, T.; Kitayama, T. *J. Appl. Phys*. **1981**, *52*, 948.
(2) Furukawa, T.; Ohuchi, M.; Chiba, A.; Date, M. *Macromolecules* **1984**, *17*, 1384.
(3) Koizumi, N.; Haikawa, N.; Habuka, H. *Ferroelectrics* **1984**, *57*, 99.
(4) Tashiro, K.; Takano, K.; Kobayashi, M.; Chatani, Y.; Tadokoro, H. *Ferroelectrics* **1984**, *57*, 297.
(5) Fernandez, M. V.; Suzuki, A.; Chiba, A. *Macromolecules* **1987**, *20*, 1806.
(6) Lovinger, A. J.; Davis, D. D.; Cais, R. E.; Kometani, J. K. *Macromolecules* **1988**, *21*, 78.
(7) Balta Calleja, F. J.; Gonzalez Arche, A.; Ezquerra, T. A.; Santa Cruz, C.; Batallan, F.; Frick, B.; Lopez Cabarcoz, E. *Adv. Polym. Sci*. **1993**, *108*, 1.
(8) Bellet-Amalric, E.; Legrand, J. F. *Eur. Phys. J. B* **1998**, *3*, 225.
(9) Yagi, T.; Teramoto, M.; Sako, J. *Polym. J*. **1980**, *12*, 209.
(10) Higashihata, Y.; Sako, J.; Yagi, T. *Ferroelectrics* **1981**, *32*, 85.
(11) Furukawa, T.; Wen, J. X.; Suzuki, K.; Takashina, Y.; Date, M. J. *Appl. Phys*. **1984**, *56*, 829.
(12) Dario, P.; de Rossi, D.; Giannotti, G.; Vivaldi, F.; Pinolli, P. C. *Ferroelectrics* **1984**, *60*, 199.
(13) Koga, K.; Ohigashi, H. *J. Appl. Phys*. **1986**, *59*, 2142.
(14) *Electrets*; Sessler, G. M., Ed.; Springer-Verlag: Berlin, 1987.
(15) Wang, H.; Zhang, Q. M.; Cross, L. E. *J. Appl. Phys*. **1993**, *74*, 3394.
(16) Ohigashi, H. In *The Applications of Ferroelectric Polymers*; Wang, T. T., Herbert, J. M., Glass, A. M., Eds.; Chapman and Hall: New York, 1988; p 237.
(17) Kimura, K.; Ohigashi, H. *Appl. Phys. Lett*. **1983**, *43*, 834.
(18) Urayama, K.; Oliver, K.; Böhmer, R.; Neher, D. *J. Appl. Phys*. **1999**, *86*, 6367.
(19) Bune, A. V.; Fridkin, V. M.; Ducharme, S.; Blinov, L. M.; Palto, S. P.; Sorokin, A. V.; Yudin, S. G.; Zlatkin, A. *Nature* **1998**, *391*, 874.
(20) Bune, A.; Ducharme, S.; Fridkin, V.; Blinov, L.; Palto, S.; Petukhova, N.; Yudin, S. *Appl. Phys. Lett*. **1995**, *67*, 3975.
(21) Ducharme, S.; Bune, A. V.; Blinov, L. M.; Fridkin, V. M.; Palto, S. P.; Sorokin, A. V.; Yudin, S. G. *Phys. Rev. B* **1998**, *57*, 25.
(22) Bune, A. V.; Zhu, C.; Decharme, S.; Blinov, L. M.; Fridkin, V. M.; Palto, S. P.; Petukhova, N. G.; Yudin, S. G. *J. Appl. Phys*. **1999**, *85*, 7869.
(23) Kimura, K.; Ohigashi, H. *Jpn. J. Appl. Phys*. **1986**, *25*, 383.
(24) Winkelhahn, H.-J.; Winter, H. H.; Neher, D. *Appl. Phys. Lett*. **1994**, *64*, 1347.
(25) Winkelhahn, H.-J.; Pakula, T.; Neher, D. *Macromolecules* **1996**, *29*, 6865.
(26) Levitus, M.; Glasser, G.; Neher, D.; Aramandia, P. F. *Chem. Phys. Lett*. **1997**, *277*, 118.
(27) Jaworek, T.; Neher, D.; Wegner, G.; Wieringa, R. H.; Schouten, A. J. *Science* **1998**, *279*, 57.
(28) Pralle, M. U.; Urayama, K.; Tew, G. N.; Neher, D.; Wegner, G.; Stupp, S. I. *Angew. Chem., Int. Ed. Engl*. **2000**, *39*, 1486.
(29) Nomarski, G. *J. Phys. Radium* **1955**, *16*, 95.
(30) Schonenberger, C.; Alvarado, S. F. *Rev. Sci. Instrum*. **1990**, *60*, 3131.
(31) Furukawa, T. *Ferroelectrics* **1984**, *57*, 63.
(32) Kittel, C. *Introduction to Solid Physics*; John Wiley & Sons: New York, 1986.
(33) Aktsipetrov, O. A.; Misuryaev, T. V.; Murzina, T. V.; Blinov, L. M.; Fridkin, V. M.; Palto, S. P. *Opt. Lett*. **2000**, *15*, 411.
(34) Koizumi, N.; Murata, Y.; Oka, Y. *Jpn. J. Appl. Phys*. **1984**, *23*, 324.
(35) Bellet-Almalric, E.; Legrand, J. F.; Stock-Schweyer, M.; Meurer, B. *Polymer* **1994**, *35*, 34.
(36) Kimura, K.; Ohigashi, H. *J. Appl. Phys*. **1987**, *61*, 4749.
(37) Ikeda, S.; Suzuki, H.; Koyama, K.; Wada, Y. *Polym. J*. **1987**, *19*, 681.
(38) Furukawa, T.; Lovinger, A. J.; Davis, G. T.; Broadhurst, M. G. *Macromolecules* **1983**, *16*, 1885.
(39) Ohigashi, H. *Jpn. J. Appl. Phys*. **1985**, *24*, 23.
(40) Palto, S.; Blinov, L.; Dubovik, E.; Fridkin, V.; Petukhova, N.; Sorokin, A.; Verkhovskya, K.; Yudin, S.; Zlatkin, A. *Europhys. Lett*. **1996**, *34*, 465.
(41) E.g.: Billmeyer, F. W. *Textbook of Polymer Science*, 3rd ed.; John Wiley & Sons: New York, 1984.
(42) Tashiro, K.; Takano, K.; Kobayashi, M.; Chatani, Y.; Tadokoro, H. *Polymer* **1984**, *25*, 195.
(43) Tashiro, K.; Takano, K.; Kobayashi, M.; Chatani, Y.; Tadokoro, H. *Ferroelectrics* **1984**, *57*, 297.
(44) Lovinger, A. J.; Davis, G. T.; Furukawa, T.; Broadhurst, M. G. *Macromolecules* **1982**, *15*, 323.
(45) Davis, G. T.; Furukawa, T.; Lovinger, A. J.; Broadhurst, M. G. *Macromolecules* **1982**, *15*, 329.

MA000855W